University of Baghdad
College of Engineering
JE
JOURNAL OF ENGINEERING

Journal of Engineering

journal homepage: www.jcoeng.edu.iq

Volume 32 Number 2 February 2026

Thermal Buckling Analysis of Laminated Composite Plates Using Four-Variable Refined Plate Theory

Ahmed Khamees Sabea *, Widad Ibraheem Majeed

Department of Mechanical Engineering, College of Engineering, University of Baghdad, Baghdad, Iraq

ABSTRACT

This paper investigates the thermal buckling of laminated composite plates based on a refined plate theory that incorporates four variables, using hyperbolic and polynomial shear strain functions for the first time to analyze thermal buckling of a laminated plate with all edges simply supported. The proposed shear function incorporates the variation of transverse shear stress over the thickness of the plate in a parabolic form and achieves zero traction on the upper and bottom surfaces of the plate without implementing a shear correction factor. Equations of motion are derived according to the principle of virtual displacement. The analytical solution is carried out using Navier's solution. The numerical results of the orthotropic properties of both cross-ply and angle-ply laminates are calculated by programming a MATLAB code. In the present study, the influence of changing various design parameters, such as aspect ratio (a/b), orthotropic ratio (E_1/E_2), thickness ratio (a/h), and thermal expansion coefficient ratio (α_2/α_1), for symmetric and antisymmetric laminated composite plates is analyzed. The results are evaluated by the assumption of uniform temperature variation through the plate, which exhibits good agreement for both thick and thin plates compared with previous studies.

Keywords: Thermal buckling, Composite plates, Refined shear theory.

1. INTRODUCTION

The broad use of laminated composite plates in modern manufacturing and technological fields, especially aerospace, automotive, and renewable energy, is due to their anisotropic, tailorable, and high-stiffness to light-weight properties, unlike traditional metals **(Elsisi et al., 2025)**. However, these benefits come with significant complexities in analysis. Many theories have been made to come up with simple yet exact analytical methods and closed-form solutions. Many applications of these laminates composite used in structures that subjected to wide variation of temperature values caused by surrounding atmosphere which affect the exposure layers of plate and causes serious stresses, to overcome this situation, it's necessary to manufacture those plates using many thin orthotropic bonded layers with

*Corresponding author
Peer review under the responsibility of University of Baghdad.
https://doi.org/10.31026/j.eng.2026.02.07

Article received: 15/11/2025
Article revised: 01/01/2026
Article accepted: 05/01/2026
Article published: 01/02/2026

varying material properties, which require precise mathematical modelling theories to account for thermal environment and its effect on those laminated plates **(Khandan et al., 2012; Odeh et al., 2024; Qian et al., 2024)**. **(Xing and Wang, 2017)** conducted a study using a Graded composite thin plate varying according to a power law through its thickness as a model to investigate the Thermal bifurcation point with a variety of boundary conditions under the influence of both linear and nonlinear temperature environments. The separation-of-variables method was applied, and a new mathematical solution was also proposed. **(Torabi et al., 2019)** adopted higher order deformation theory for investigating thermal buckling for a different shape of nanotube reinforced composite (FG-CNTRC) plates influenced by thermal loads, considering material thermo-mechanical properties affected by temperature. **(Abdulrazzaq et al., 2020)** investigated thermo-elastic buckling of small-scale functionally graded material (FGM) nano-size plates with clamped edge conditions resting on an elastic substrate, subjected to both linear and non-linear temperature distributions. In the study, the FGM had an exponential gradient across its thickness. **(Daikh et al., 2020)** applied TOT in the study of thermal buckling and natural vibration of single-walled carbon nanotubes reinforced laminates using (FGM). A study by **(Nguyen et al., 2020)** developed a new higher-order shear deformation theory and used a novel exponential shape function within the Ritz method. The effect of geometrical nonlinearities due to pressure load on the thermal buckling and dynamic characteristics of composite plates using (FSDT) was investigated by **(Yang et al., 2020)**. Based on five variables, the refined plate theory based on parabolic form shape function **(Hashim and Sadiq, 2021)** conducted a study to investigate thermal buckling. **(Li et al., 2021)** carried out a thermomechanical buckling analysis of sandwich plates using four variables, the shear deformation theory of (FGM). The optimization study of design and control of thermal buckling of piezoelectric fibre reinforced composite actuators using four variable shear deformation theory and accounting for stress variation through thickness by a trigonometric function was conducted by **(Xue et al., 2021)**. **(Yahea and Majeed, 2021)** studied thermal buckling of (SS) cross and angle composite plate in the framework of four variable trigonometric functions. Modern studies, such as the work of **(Anandan et al., 2022)** uses models of composite plates reinforced by natural fibres like Flax and test them numerically under thermal loads according to finite element analysis runs in ANSYS Workbench. Another approach is the use of (FSDT) in the process of analysing thermal buckling of reinforced laminated composite plates with cutouts using level sets, a novel method evolved by **(Devarajan and Kapania, 2022)**.

(Hajlaoui and Dammak, 2022) investigated thermal post-buckling of (FG) plates with two material properties based on temperature decency (dependent and independent) in three-dimensional coordinates through the use of a modified first-order enhanced solid shell element. The work of **(Ma and Jin, 2022)** focused on the analysis of the thermal buckling of graphene-reinforced composite (FG-GRC) laminated thick plates using the seven-unknown theory. A study by **(Kareem, 2024; Majeed and Sadiq, 2022)** developed thermal buckling analyses of laminated plates based on improved higher-order shape functions with parameter ''m''; the improvement extends the theory to mathematically modelling thin and thick plates. **(Miglani et al., 2022)** investigated the bending and buckling of composite plates due to thermal load using high-order shear deformation theory of a six-variable quasi-3D model. The use of high-order shear deformation theory to represent the effect of thermal buckling on porous thick rectangular plates made of FGM was conducted by **(Saad and Hadji, 2022)**. **(Varelis and Saravanos, 2022)** presented a nonlinear model for

piezoelectric laminated plates that couples thermal, electrical, and mechanical fields. Using a developed finite element, it quantifies how pyroelectric and piezoelectric effects impact thermal buckling and the nonlinear response of smart composite plates under different temperature conditions. Thermal buckling analyses of cylindrical micro shells made of (FGM) were conducted by **(Mehditabar et al., 2023)** using classical high-order shear deformation theory. A study by **(Moradi Haghighi and Alibeigloo, 2023)** was conducted on rectangular carbon nanotubes using third-order shear deformation theory to investigate thermal buckling and free vibration of (FGM) Further application of high-order theories utilized by **(Bracaglia et al., 2024)** in the thermal buckling of Variable Angle Tow (VAT) composite plates, assuming linear pre-buckling, proposes linear eigenvalue analysis. **(Majeed and Sadiq, 2025)** proposed the same theory and the same shape function used in this paper, but to investigate the mechanical buckling of rectangular laminated plates with all supported edges.

In the present work function, is used to investigate thermal buckling of both cross-ply and angle-ply laminated plate for the first time, which is a combination of hyperbolic and polynomial and this shape function satisfies the zero strain on the free surfaces of the plate without the need for shear correction factor, also has only four unknown variables, which are less than variables used by high order shear deformation. The governing equations of motion are derived from Hamilton's principle of total potential energy and solved for simply supported boundary conditions using the Navier series. The accuracy of the results was validated by comparing them to other results from different theories.

2. THEORY AND FORMULATION

In the present study formulation of the problem considers a composite plate subjected to a system of in-plane compressive loads due to thermal effects.

2.1 Kinematics

Based on the work of **(Ebrahimi et al., 2021)**, the displacement field of the model is represented as :

$$u_{(x,y,z)} = u_{0_{(x,y)}} + z\left(-\frac{\partial w^b}{\partial x}\right) + F(z)\left(-\frac{\partial w^s}{\partial x}\right) \quad (1)$$

$$v_{(x,y,z)} = v_{0_{(x,y)}} + z\left(-\frac{\partial w^b}{\partial y}\right) + F(z)\left(-\frac{\partial w^s}{\partial y}\right) \quad (2)$$

$$w_{(x,y,z)} = w^b{}_{(x,y)} + w^s{}_{(x,y)} \quad (3)$$

Where u_0, v_0, w^b, and w^s are the four displacement components, F(z) represents the shape function, which describes the transverse shear stress through the thickness, achieving zero stress at the free edges of the plate. For the present study, it was described according to **(Kada and Abdelouahed, 2022)** as below:

$$F(z) = z - h\left(\sinh\left(\frac{z}{h}\right)\right) + \left(\left(\frac{4z^3}{3h^2}\right)\cosh(0.5)\right) \quad (4)$$

2.2 Strain Relations

Formulating the linear strain-displacement relations correlated to the displacement field **(Reddy, 2003)** just as:

$$\begin{Bmatrix}\varepsilon_{xx}\\ \varepsilon_{yy}\\ \gamma_{xy}\end{Bmatrix}=\begin{Bmatrix}\varepsilon^0_{xx}\\ \varepsilon^0_{xx}\\ \gamma^0_{xy}\end{Bmatrix}+z\begin{Bmatrix}\varepsilon^1_{xx}\\ \varepsilon^1_{xx}\\ \gamma^1_{xy}\end{Bmatrix}+F(z)\begin{Bmatrix}\varepsilon^2_{xx}\\ \varepsilon^2_{yy}\\ \gamma^2_{xy}\end{Bmatrix} \quad (5)$$

Where:

$$\varepsilon_{ij}=\frac{1}{2}\left(U_{i,j}+U_{j,i}\right) \quad (6)$$

$$\begin{Bmatrix}\gamma_{yz}\\ \gamma_{xz}\end{Bmatrix}=\begin{Bmatrix}\gamma^0_{yz}\\ \gamma^0_{yz}\end{Bmatrix}+F'(z)\begin{Bmatrix}\gamma^3_{yz}\\ \gamma^3_{yz}\end{Bmatrix} \quad (7)$$

$$\begin{Bmatrix}\gamma_{yz}\\ \gamma_{xz}\end{Bmatrix}=g(z)\begin{Bmatrix}\frac{\partial w^s}{\partial y}\\ \frac{\partial w^s}{\partial x}\end{Bmatrix} \quad (8)$$

Where:

$$g(z)=1-F'(z)=\cosh\left(\frac{z}{h}\right)+\left(\frac{4z^2}{h^2}\right)\cosh(0.5) \quad (9)$$

$$\varepsilon_{zz}=0 \quad (10)$$

2.3 Equations of Motion

This section applies the Hamilton principle to formulate the governing equations of motion.

$$0=\int_{\Omega_0}^{k}(\delta U+\delta V)dv \quad (11)$$

Where δU and δV are Virtual strain energy and Virtual external work done due to thermal effect, respectively.

$$\delta U=\int_{\Omega_0}^{K}\int_{z_k}^{z_{k+1}}\left[\begin{Bmatrix}\sigma_{xx}\\ \sigma_{yy}\\ \sigma_{xy}\end{Bmatrix}\begin{Bmatrix}\delta\varepsilon_{xx}\\ \delta\varepsilon_{yy}\\ \delta\gamma_{xy}\end{Bmatrix}^k+\begin{Bmatrix}\sigma_{yz}\\ \sigma_{xz}\end{Bmatrix}\begin{Bmatrix}\delta\gamma_{yz}\\ \delta\gamma_{xz}\end{Bmatrix}^k\right]dzdxdy \quad (12)$$

$$\delta U=\int_{\Omega_0}^{K}\left[\begin{Bmatrix}N_{xx}\\ N_{yy}\\ N_{xy}\end{Bmatrix}\begin{Bmatrix}\delta\varepsilon^0_{xx}\\ \delta\varepsilon^0_{yy}\\ \delta\gamma^0_{xy}\end{Bmatrix}^k+\begin{Bmatrix}M^b_{xx}\\ M^b_{yy}\\ M^b_{xy}\end{Bmatrix}\begin{Bmatrix}\delta\varepsilon^1_{xx}\\ \delta\varepsilon^1_{yy}\\ \delta\gamma^1_{xy}\end{Bmatrix}^k+\begin{Bmatrix}M^s_{xx}\\ M^s_{yy}\\ M^s_{xy}\end{Bmatrix}\begin{Bmatrix}\delta\varepsilon^2_{xx}\\ \delta\varepsilon^2_{yy}\\ \delta\gamma^2_{xy}\end{Bmatrix}^k+\begin{Bmatrix}Q_y\\ Q_x\end{Bmatrix}\begin{Bmatrix}\delta\gamma^0_{yz}\\ \delta\gamma^0_{xz}\end{Bmatrix}^k\right]dxdy \quad (13)$$

$$\delta U=\int_{\Omega o}^{k}\left[\begin{Bmatrix}N_{xx}\\ N_{yy}\\ N_{xy}\end{Bmatrix}\begin{Bmatrix}\frac{\partial\delta u_0}{\partial x}\\ \frac{\partial\delta v_0}{\partial y}\\ \frac{\partial\delta u_0}{\partial y}+\frac{\partial\delta v_0}{\partial x}\end{Bmatrix}^k-\begin{Bmatrix}M^b_{xx}\\ M^b_{yy}\\ M^b_{xy}\end{Bmatrix}\begin{Bmatrix}\frac{\partial^2\delta w^b}{\partial x^2}\\ \frac{\partial^2\delta w^b}{\partial y^2}\\ 2\frac{\partial^2 w^b}{\partial x\partial y}\end{Bmatrix}^k-\begin{Bmatrix}M^s_{xx}\\ M^s_{yy}\\ M^s_{xy}\end{Bmatrix}\begin{Bmatrix}\frac{\partial^2\delta w^s}{\partial x^2}\\ \frac{\partial^2\delta w^s}{\partial y^2}\\ 2\frac{\partial^2\delta w^s}{\partial x\partial y}\end{Bmatrix}^k+\begin{Bmatrix}Q_y\\ Q_x\end{Bmatrix}\begin{Bmatrix}\frac{\partial\delta w^s}{\partial y}\\ \frac{\partial\delta w^s}{\partial x}\end{Bmatrix}^k\right]dxdy \quad (14)$$

Where:

$$\left(N_i,M^b_i,M^s_i\right)=\sum_{k=1}^{N}\int_{z_k}^{z_{k+1}}\sigma^k_i\left(1,z,F(z)\right)dz \quad , \quad i=(xx,yy,xy) \quad (15)$$

$$\left(Q_j\right)=\sum_{k=1}^{N}\int_{z_k}^{z_{k+1}}\sigma^k_{jz}\,g(z)dz \quad , \quad j=(y,x) \quad (16)$$

$$\delta V=-\frac{1}{2}\int_{\Omega_0}^{K}\left[\begin{Bmatrix}N^{\top}_{xx}\\ N^{\top}_{yy}\\ N^{\top}_{xy}\end{Bmatrix}\delta\begin{Bmatrix}\left(\frac{\partial w}{\partial x}\right)^2\\ \left(\frac{\partial w}{\partial y}\right)^2\\ \left(\frac{\partial w}{\partial x}\frac{\partial w}{\partial y}\right)\end{Bmatrix}^k\right]dxdy \quad (17)$$

$$\delta V = -\frac{1}{2}\int_{\Omega_0}^{K}\left[\begin{Bmatrix}N_{xx}^{\top}\\N_{yy}^{\top}\\N_{xy}^{\top}\end{Bmatrix}\begin{Bmatrix}2\left(\frac{\partial w}{\partial x}\right)\left(\frac{\partial \delta w}{\partial x}\right)\\2\left(\frac{\partial w}{\partial y}\right)\left(\frac{\partial \delta w}{\partial y}\right)\\\left(\frac{\partial \delta w}{\partial x}\frac{\partial w}{\partial y}\right)+\left(\frac{\partial w}{\partial x}\frac{\partial \delta w}{\partial y}\right)\end{Bmatrix}^{k}\right]dxdy \tag{18}$$

$$\delta V = -\int_{\Omega_0}^{k}\left[\begin{Bmatrix}N_{xx}^{\top}\\N_{yy}^{\top}\\N_{xy}^{\top}\end{Bmatrix}\begin{Bmatrix}\left(\frac{\partial(w^b+w^s)}{\partial x}\right)\left(\frac{\partial(\delta w^b+\delta w^s)}{\partial x}\right)\\\left(\frac{\partial(w^b+w^b)}{\partial y}\right)\left(\frac{\partial(\delta w^b+\delta w^s)}{\partial y}\right.\\\frac{\partial(\omega^b+\omega^s)}{\partial y}\frac{\partial(\delta\omega^b+\delta\omega^s)}{\partial x}+\frac{\partial(\omega^b+\omega^s)}{\partial x}\frac{\partial(\delta\omega^b+\delta\omega^s)}{\partial y}\end{Bmatrix}^{k}\right]dxdy \tag{19}$$

Where (w) is assumed to be the algebraic sum of the deflection caused by bending and shear modes through the thickness of the plate **(Ebrahimi et al., 2021)**.

$$\begin{Bmatrix}N_{xx}^{\top}\\N_{yy}^{\top}\\N_{xy}^{\top}\end{Bmatrix}=\sum_{k=1}^{N}\int_{Z_k}^{Z_{k+1}}\begin{bmatrix}\bar{Q}_{11}&\bar{Q}_{12}&\bar{Q}_{16}\\\bar{Q}_{12}&\bar{Q}_{22}&\bar{Q}_{26}\\\bar{Q}_{16}&\bar{Q}_{26}&\bar{Q}_{66}\end{bmatrix}\begin{Bmatrix}\alpha_{xx}\\\alpha_{yy}\\2\alpha_{xy}\end{Bmatrix}\Delta T cr\, dz \tag{20}$$

substituting Eqs. (14) and (19) into Eq. (11), integrating by parts and using divergence theory, then setting coefficients of (δu_0, δv_0, δw^b, δw^s) to zero to evaluate governing equations as below:

$$\delta u_0: \quad \frac{\partial N_{xx}}{\partial x}+\frac{\partial N_{xy}}{\partial y}=0 \tag{21}$$

$$\delta v_0: \quad \frac{\partial N_{yy}}{\partial y}+\frac{\partial N_{xy}}{\partial x}=0 \tag{22}$$

$$Sw^b:\left(\frac{\partial^2 M_{xx}^b}{\partial x^2}+\frac{\partial^2 M_{yy}^b}{\partial y^2}+2\frac{\partial^2 M_{xy}^b}{\partial x\partial y}\right)+\left(N_{xx}^T\frac{\partial^2(w^b+w^s)}{\partial x^2}+N_{yy}^T\frac{\partial^2(w^b+w^s)}{\partial y^2}+2N_{xy}^T\frac{\partial^2(w^b+w^s)}{\partial x\partial y}\right)=0 \tag{23}$$

$$\delta w^s: \quad \left(\frac{\partial^2 M_{xx}^s}{\partial x^2}+\frac{\partial^2 M_{yy}^s}{\partial y^2}+2\frac{\partial^2 M_{xy}^s}{\partial x\partial y}+\frac{\partial Q_y}{\partial y}+\frac{\partial Q_x}{\partial x}\right)+\left(N_{xx}^{\top}\frac{\partial^2(w^b+w^s)}{\partial x^2}+N_{yy}^{\top}\frac{\partial^2(w^b+w^s)}{\partial y^2}+\right.$$
$$\left.2N_{xy}^{\top}\frac{\partial^2(w^b+w^s)}{\partial x\partial y}\right)=0 \tag{24}$$

2.4 Constitutive Equations

Based on linear solids' constitutive equations, elastic stress-strain relationships are represented. **(Ebrahimi et al., 2021)**.

$$Q_{11}=\frac{E_1}{1-v_{12}v_{21}}\ ,\ Q_{12}=\frac{v_{12}E_2}{1-v_{12}v_{21}}\ ,\ Q_{22}=\frac{E_2}{1-v_{12}v_{21}} \tag{25}$$

$$Q_{66}=G_{12}\quad ,\quad Q_{44}=G_{23}\ ,\quad Q_{55}=G_{13} \tag{26}$$

Where G_{ij}, E_{ij} and v_{ij}, are the shear modulus, Young's modulus, and Poisson's ratio of the plate in different planes.

$$\begin{Bmatrix}\sigma_1\\\sigma_2\\\sigma_3\end{Bmatrix}=\begin{bmatrix}Q_{11}&Q_{12}&0\\Q_{12}&Q_{22}&0\\0&0&Q_{66}\end{bmatrix}\begin{Bmatrix}\varepsilon_1\\\varepsilon_2\\\varepsilon_3\end{Bmatrix} \tag{27}$$

$$\begin{Bmatrix}\sigma_4\\\sigma_5\end{Bmatrix}=\begin{bmatrix}Q_{44}&0\\0&Q_{55}\end{bmatrix}\begin{Bmatrix}\varepsilon_4\\\varepsilon_5\end{Bmatrix} \tag{28}$$

$$\begin{Bmatrix}\sigma_{xx}\\ \sigma_{yy}\\ \sigma_{xy}\end{Bmatrix}=\begin{bmatrix}\bar{Q}_{11} & \bar{Q}_{12} & \bar{Q}_{16}\\ \bar{Q}_{12} & \bar{Q}_{22} & \bar{Q}_{26}\\ \bar{Q}_{16} & \bar{Q}_{26} & \bar{Q}_{66}\end{bmatrix}\begin{Bmatrix}\varepsilon_{xx}\\ \varepsilon_{yy}\\ \gamma_{xy}\end{Bmatrix} \tag{29}$$

$$\begin{Bmatrix}N_{xx}\\ N_{yy}\\ N_{xy}\end{Bmatrix}=\begin{bmatrix}A_{11} & A_{12} & A_{16}\\ A_{12} & A_{22} & A_{26}\\ A_{16} & A_{26} & A_{66}\end{bmatrix}\begin{Bmatrix}\varepsilon^0_{xx}\\ \varepsilon^0_{yy}\\ \gamma^0_{xy}\end{Bmatrix}+\begin{bmatrix}B_{11} & B_{12} & B_{16}\\ B_{12} & B_{22} & B_{26}\\ B_{16} & B_{26} & B_{66}\end{bmatrix}\begin{Bmatrix}\varepsilon^1_{xx}\\ \varepsilon^1_{yy}\\ \gamma^1_{xy}\end{Bmatrix}+\begin{bmatrix}E_{11} & E_{12} & E_{16}\\ E_{12} & E_{22} & E_{26}\\ E_{16} & E_{26} & E_{66}\end{bmatrix}\begin{Bmatrix}\varepsilon^2_{xx}\\ \varepsilon^2_{yy}\\ \gamma^2_{xy}\end{Bmatrix} \tag{30}$$

$$\begin{Bmatrix}M^b_{xx}\\ M^b_{yy}\\ M^b_{xy}\end{Bmatrix}=\begin{bmatrix}B_{11} & B_{12} & B_{16}\\ B_{12} & B_{22} & B_{26}\\ B_{16} & B_{26} & B_{66}\end{bmatrix}\begin{Bmatrix}\varepsilon^0_{xx}\\ \varepsilon^0_{yy}\\ \gamma^0_{xy}\end{Bmatrix}+\begin{bmatrix}D_{11} & D_{12} & D_{16}\\ D_{12} & D_{22} & D_{26}\\ D_{16} & D_{26} & D_{66}\end{bmatrix}\begin{Bmatrix}\varepsilon^1_{xx}\\ \varepsilon^1_{yy}\\ \gamma^1_{xy}\end{Bmatrix}+\begin{bmatrix}F_{11} & F_{12} & F_{16}\\ F_{12} & F_{22} & F_{26}\\ F_{16} & F_{26} & F_{66}\end{bmatrix}\begin{Bmatrix}\varepsilon^2_{xx}\\ \varepsilon^2_{yy}\\ \gamma^2_{xy}\end{Bmatrix} \tag{31}$$

$$\begin{Bmatrix}M^s_{xx}\\ M^s_{yy}\\ M^s_{xy}\end{Bmatrix}=\begin{bmatrix}E_{11} & E_{12} & E_{16}\\ E_{12} & E_{22} & E_{26}\\ E_{16} & E_{26} & E_{66}\end{bmatrix}\begin{Bmatrix}\varepsilon^0_{xx}\\ \varepsilon^0_{yy}\\ \gamma^0_{xy}\end{Bmatrix}+\begin{bmatrix}F_{11} & F_{12} & F_{16}\\ F_{12} & F_{22} & F_{26}\\ F_{16} & F_{26} & F_{66}\end{bmatrix}\begin{Bmatrix}\varepsilon^1_{xx}\\ \varepsilon^1_{yy}\\ \gamma^1_{xy}\end{Bmatrix}+\begin{bmatrix}H_{11} & H_{12} & H_{16}\\ H_{12} & H_{22} & H_{26}\\ H_{16} & H_{26} & H_{66}\end{bmatrix}\begin{Bmatrix}\varepsilon^2_{xx}\\ \varepsilon^2_{yy}\\ \gamma^2_{xy}\end{Bmatrix} \tag{32}$$

$$\begin{Bmatrix}Q_y\\ Q_x\end{Bmatrix}=\begin{bmatrix}L_{44} & L_{45}\\ L_{45} & L_{55}\end{bmatrix}\begin{Bmatrix}\gamma^0_{yz}\\ \gamma^0_{xz}\end{Bmatrix} \tag{33}$$

$$(A_{ij},B_{ij},D_{ij},E_{ij},F_{ij},H_{ij})=\int_{z_k}^{z_{k+1}}\bar{Q}_{ij}(1,z,z^2,F(z),z\cdot F(z),(F(z))^2)dz\,,i=(1,2,6) \tag{34}$$

$$L_{ij}=\int_{z_k}^{k_{k+1}}\bar{Q}_{ij}(g(z))^2dz \quad , \quad i,j=(4,5) \tag{35}$$

2.5 Equations of Motion in Terms of Displacements

Substituting Eqs. (30) to (33) into Eqs. (21) to (2) to depict the governing equations **(Reddy, 2003)**:

$$A_{11}\left(\frac{\partial^2u_0}{\partial x^2}\right)+2A_{16}\left(\frac{\partial^2u_0}{\partial x\partial y}\right)+A_{66}\left(\frac{\partial^2u_0}{\partial y^2}\right)+A_{16}\left(\frac{\partial^2v_0}{\partial x^2}\right)+(A_{12}+A_{66})\left(\frac{\partial^2v_0}{\partial x\partial y}\right)A_{11}\left(\frac{\partial^2u_0}{\partial x^2}\right)+$$
$$2A_{16}\left(\frac{\partial^2u_0}{\partial x\partial y}\right)+A_{66}\left(\frac{\partial^2u_0}{\partial y^2}\right)+A_{16}\left(\frac{\partial^2v_0}{\partial x^2}\right)+(A_{12}+A_{66})\left(\frac{\partial^2v_0}{\partial x\partial y}\right)+A_{26}\left(\frac{\partial^2v_0}{\partial y^2}\right)-B_{11}\left(\frac{\partial^3w^b}{\partial x^3}\right)-$$
$$3B_{16}\left(\frac{\partial^3w^b}{\partial x^2\partial y}\right)-(B_{12}+2B_{66})\left(\frac{\partial^3w^b}{\partial x\partial y^2}\right)-B_{26}\left(\frac{\partial^3w^b}{\partial y^3}\right)-3E_{16}\left(\frac{\partial^3w^s}{\partial x^2\partial y}\right)-(E_{12}+2E_{66})\left(\frac{\partial^3w^s}{\partial x\partial y^2}\right)-$$
$$E_{26}\left(\frac{\partial^3w^s}{\partial y^3}\right)=0 \tag{36}$$

$$A_{16}\left(\frac{\partial^2u_0}{\partial x^2}\right)+(A_{12}+A_{66})\left(\frac{\partial^2u_0}{\partial x\partial y}\right)+A_{26}\left(\frac{\partial^2u_0}{\partial y^2}\right)+A_{66}\left(\frac{\partial^2v_0}{\partial x^2}\right)+2A_{26}\left(\frac{\partial^2v_0}{\partial x\partial y}\right)+A_{22}\left(\frac{\partial^2v_0}{\partial y^2}\right)-$$
$$B_{16}\left(\frac{\partial^3w^b}{\partial x^3}\right)-(B_{12}+2B_{66})\left(\frac{\partial^3w^b}{\partial x^2\partial y}\right)-3B_{26}\left(\frac{\partial^3w^b}{\partial x\partial y^2}\right)-B_{22}\left(\frac{\partial^3w^b}{\partial y^3}\right)-E_{16}\left(\frac{\partial^3w^s}{\partial x^3}\right)-$$
$$(E_{12}+2E_{66})\left(\frac{\partial^3w^s}{\partial x^2\partial y}\right)-3E_{26}\left(\frac{\partial^3w^s}{\partial x\partial y^2}\right)-E_{22}\left(\frac{\partial^3w^s}{\partial y^3}\right)=0 \tag{37}$$

$$B_{11}\left(\frac{\partial^3u_0}{\partial x^3}\right)+3B_{16}\left(\frac{\partial^3u_0}{\partial x^2\partial y}\right)+(B_{12}+2B_{66})\left(\frac{\partial^3u_0}{\partial x\partial y^2}\right)+B_{26}\left(\frac{\partial^3u_0}{\partial y^3}\right)+B_{16}\left(\frac{\partial^3v_0}{\partial x^3}\right)+$$
$$(B_{12}+2B_{66})\left(\frac{\partial^3v_0}{\partial x^2\partial y}\right)+3B_{26}\left(\frac{\partial^3v_0}{\partial x\partial y^2}\right)+B_{22}\left(\frac{\partial^3v_0}{\partial y^3}\right)-D_{11}\left(\frac{\partial^4w^b}{\partial x^4}\right)-4D_{16}\left(\frac{\partial^4w^b}{\partial x^3\partial y}\right)-$$
$$2(D_{12}+2D_{66})\left(\frac{\partial^4w^b}{\partial x^2\partial y^2}\right)-4D_{26}\left(\frac{\partial^4w^b}{\partial x\partial y^3}\right)-D_{22}\left(\frac{\partial^4w^b}{\partial y^4}\right)-F_{11}\left(\frac{\partial^4w^s}{\partial x^4}\right)-4F_{16}\left(\frac{\partial^4w^s}{\partial x^3\partial y}\right)-$$
$$2(F_{12}+2F_{66})\left(\frac{\partial^4w^s}{\partial x^2\partial y^2}\right)-4F_{26}\left(\frac{\partial^4w^s}{\partial x\partial y^3}\right)-F_{22}\left(\frac{\partial^4w^s}{\partial y^4}\right)+N^{\top}_{xx}\left(\frac{\partial^2w^b}{\partial x^2}\right)+N^{\top}_{xx}\left(\frac{\partial^2w^s}{\partial x^2}\right)+$$
$$N^{\top}_{yy}\left(\frac{\partial^2w^b}{\partial y^2}\right)+N^{\top}_{yy}\left(\frac{\partial^2w^s}{\partial y^2}\right)+2N^{\top}_{xy}\left(\frac{\partial^2w^b}{\partial x\partial y}\right)+2N^{\top}_{xy}\left(\frac{\partial^2w^s}{\partial x\partial y}\right)=0 \tag{38}$$

$$E_{11}\left(\frac{\partial^3 u_0}{\partial x^3}\right)+3E_{16}\left(\frac{\partial^3 u_0}{\partial x^2\partial y}\right)+(E_{12}+2E_{66})\left(\frac{\partial^3 u_0}{\partial x\partial y^2}\right)+E_{26}\left(\frac{\partial^3 u_0}{\partial y^3}\right)+E_{16}\left(\frac{\partial^3 v_0}{\partial x^3}\right)+$$
$$(E_{12}+2E_{66})\left(\frac{\partial^3 v_0}{\partial x^2\partial y}\right)+3E_{26}\left(\frac{\partial^3 v_0}{\partial x\partial y^2}\right)+E_{22}\left(\frac{\partial^3 v_0}{\partial y^3}\right)-F_{11}\left(\frac{\partial^4 w^b}{\partial x^4}\right)-4F_{16}\left(\frac{\partial^4 w^b}{\partial x^3\partial y}\right)-$$
$$2(F_{12}+2F_{66})\left(\frac{\partial^4 w^b}{\partial x^2\partial y^2}\right)-4F_{26}\left(\frac{\partial^4 w^b}{\partial x\partial y^3}\right)-F_{22}\left(\frac{\partial^4 w^b}{\partial y^4}\right)-H_{11}\left(\frac{\partial^4 w^s}{\partial x^4}\right)-4H_{16}\left(\frac{\partial^4 w^s}{\partial x^3\partial y}\right)-$$
$$2(H_{12}+2H_{66})\left(\frac{\partial^4 w^s}{\partial x^2\partial y^2}\right)-4H_{26}\left(\frac{\partial^4 w^s}{\partial x\partial y^3}\right)-H_{22}\left(\frac{\partial^4 w^s}{\partial y^4}\right)+L_{55}\left(\frac{\partial^2 w^s}{\partial x^2}\right)+2L_{45}\left(\frac{\partial^2 w^s}{\partial x\partial y}\right)+$$
$$L_{44}\left(\frac{\partial^2 w^s}{\partial y^2}\right)+N_{xx}^{\top}\left(\frac{\partial^2 w^b}{\partial x^2}\right)+N_{xx}^{\top}\left(\frac{\partial^2 w^s}{\partial x^2}\right)+N_{yy}^{\top}\left(\frac{\partial^2 w^b}{\partial y^2}\right)+N_{yy}^{\top}\left(\frac{\partial^2 w^s}{\partial y^2}\right)+2N_{xy}^{\top}\left(\frac{\partial^2 w^b}{\partial x\partial y}\right)+$$
$$2N_{xy}^{\top}\left(\frac{\partial^2 w^s}{\partial x\partial y}\right)=0 \quad (39)$$

2.6 Analytical Solution

The simply supported boundary conditions of the composite plate model were implemented to evaluate the analytical solution of the governing equations based on Navier's method, so the following expansions of displacements have been assumed for cross-ply and angle-ply laminates, respectively **(Ebrahimi et al., 2021)**:

$$at\ x=0\ and\ x=a: v_0=w_b=w_s=M_x^b=M_x^s=0 \quad (40)$$
$$at\ y=0\ and\ y=a: u_0=w_b=w_s=M_y^s=M_y^s=0 \quad (41)$$
$$u_0(x,y,t)=\sum_{n=1}^{\infty}\sum_{m=1}^{\infty}U_{mn}cos\ \alpha xsin\ \beta y \quad (42)$$
$$v_0(x,y,t)=\sum_{n=1}^{\infty}\sum_{m=1}^{\infty}V_{mn}sin\ \alpha xcos\ \beta y \quad (43)$$
$$w^b(x,y,t)=\sum_{n=1}^{\infty}\sum_{m=1}^{\infty}W_{mn}^b sin\ \alpha xsin\ \beta y \quad (44)$$
$$w^s(x,y,t)=\sum_{n=1}^{\infty}\sum_{m=1}^{\infty}W_{mn}^s sin\ \alpha xsin\ \beta y \quad (45)$$
$$at\ x=0\ and\ x=a: u_0=w_b=w_s=M_x^b=M_x^s=0 \quad (46)$$
$$at\ y=0\ and\ y=a: v_0=w_b=w_s=M_y^s=M_y^s=0 \quad (47)$$
$$u_0(x,y,t)=\sum_{n=1}^{\infty}\sum_{m=1}^{\infty}U_{mn}sin\ \alpha xcos\ \beta y \quad (48)$$
$$v_0(x,y,t)=\sum_{n=1}^{\infty}\sum_{m=1}^{\infty}V_{mn}cos\ \alpha xsin\ \beta y \quad (49)$$
$$w^b(x,y,t)=\sum_{n=1}^{\infty}\sum_{m=1}^{\infty}W_{mn}^b sin\ \alpha xsin\ \beta y \quad (50)$$
$$w^s(x,y,t)=\sum_{n=1}^{\infty}\sum_{m=1}^{\infty}W_{mn}^s sin\ \alpha xsin\ \beta y \quad (51)$$

2.7 Thermal Buckling Analysis

Inserting Eqs. (42) to (4) and Eqs. (48) to (5) into Eqs. (3) to (39), The eigenvalue problem for cross-ply and angle-ply is formulated, respectively **(Yahea and Majeed, 2021)**:

$$\begin{Bmatrix} K_{11} & K_{12} & K_{13} & K_{14} \\ K_{12} & K_{22} & K_{23} & K_{24} \\ K_{13} & K_{23} & K_{33}-\left(N_{xx}^T\alpha^2+N_{yy}^T\beta^2\right)\Delta T & K_{34}-\left(N_{xx}^T\alpha^2+N_{yy}^T\beta^2\right)\Delta T \\ K_{14} & K_{24} & K_{34}-\left(N_{xx}^T\alpha^2+N_{yy}^T\beta^2\right)\Delta T & K_{44}-\left(N_{xx}^T\alpha^2+N_{yy}^T\beta^2\right)\Delta T \end{Bmatrix}\begin{Bmatrix} U_{mn} \\ V_{mn} \\ W_{mn}^b \\ W_{mn}^s \end{Bmatrix}=\begin{Bmatrix} 0 \\ 0 \\ 0 \\ 0 \end{Bmatrix} \quad (52)$$

3. RESULTS AND DISCUSSION

In the present study, hyperbolic and polynomial shape functions **(Kada and Abdelouahed, 2022)** are used for the first time in thermal buckling analysis of laminated composite plates based on a four-variable refined theory. The numerical result was evaluated by programming a code for MATLABR2024a software to compute the critical buckling

temperature. Two types of laminated schemes (cross and angle) were investigated for two types of plate shapes (square and rectangular).

3.1 Validation of Results

Numerical values of Critical buckling temperature are computed based on changing various parameters such as thickness ratio (a/h), aspect ratio (a/b), orthotropic ratio (E_1/E_2), and thermal expansion coefficient ratio (α_2/α_1), and compared with previous study results of the same field, showing good agreement.

3.1.1 Model Material Constants

Three models of material constants are to be used as follows **(Yahea and Majeed, 2021)**:
Material 1: $E_1/E_2=25$, $G_{12}=G_{13}=0.5E_2$, $G_{23}=0.2E_2$, $\nu_{12}=0.25$, $\alpha_2/\alpha_1=3$, $E_2=1$Gpa, $\alpha_1=1$.
Material 2: $E_1/E_0=30$, $E_2/E_0=1$, $G_{12}=G_{13}=0.65E_0$, $G_{23}=0.639E_0$, $\nu_{12}=0.21$, $\alpha_2/\alpha_0=16$, $\alpha_1/\alpha_0=-0.21$, $E_0=10$Gpa, $\alpha_0=10^{-6}$.
Material 3: $E_1/E_0=15$, $G_{12}=G_{13}=0.5E_0$, $G_{23}=0.3356$, $\nu_{12}=0.3$, $\alpha_2/\alpha_0=1$, $\alpha_1/\alpha_0=0.015$, $E_0=1$Gpa, $\alpha_0=10^{-6}$.

3.1.2 Cross-Ply Composite Plates

Numerical findings of normalized critical buckling temperature on the form ($\Delta Tcr=T^*a^2*h/\pi^2*D_{22}$) and using material 1 for **Table 1**, while using material 3 for (**Table 2** to **4**) and nondimensional critical temperature ($\Delta Tcr=T^*\alpha_0$) as follows **(Yahea and Majeed, 2021)**.
Critical temperature evaluated in **Table 1** The cross-ply laminate plate is compared with the results from previous studies. In this analysis, a symmetric scheme of laminates is used for a square composite plate. The numerical values of (ΔTcr) obtained based on this study showed good agreement with other theories, and it is closer to those obtained from (**TSDT[2]**) for both thick and thin plates. It also shows the effect of the number of layers and thickness on the critical buckling temperature. The increase in laminates produces an increase in buckling critical temperature; furthermore, as thickness increases, (ΔTcr) decreases due to diminution in stiffness (the reverse results due to dividing (ΔTcr) by D_{22}).

Table 1. Dimensionless buckling temperature (ΔTcr) of a square simply supported plate cross-ply scheme for various values of thickness ratios (a/h) **(Shu and Sun, 1994**;**Yahea and Majeed, 2021)**

Lay-up	a/h	TOT[1]	RPT	TSDT[2]	Present
$(0/90)_s$	4	0.0575	0.07115	0.07155	0.071150
	10	0.1522	0.17492	0.175	0.174918
	100	0.2435	0.24405	0.244	0.244050
	1000	0.245	0.2451	0.245	0.245023
$(0/90)_{2s}$	4	0.0315	0.03348	0.03367	0.033482
	10	0.0797	0.08231	0.08237	0.082314
	100	0.1148	0.11485	0.11484	0.114847
	1000	0.1153	0.11530	0.1153	0.115305
$(0/90)_{5s}$	4	0.0247	0.02541	0.02555	0.025411
	10	0.0621	0.06247	0.06251	0.062471
	100	0.0872	0.08716	0.08716	0.087161
	1000	0.0875	0.08759	0.08750	0.087508

Based on the numerical values of (ΔTcr) evaluated in **Table 2**. which explains the correlation of (ΔTcr) with both aspect ratios (a/b) and thickness ratio (a/h), for both symmetric and antisymmetric laminated plates. (ΔTcr) decreases when (a/h) increases, due to thickness reduction. On the other hand, (ΔTcr) increases when (a/b) increases, referring to stiffness changes when changing these design parameters.

Table 3 shows the correlation between the normalized critical buckling temperature with both different thermal expansion coefficient ratios (α_2/α_1) and thickness ratio (a/h). Results revealed that the increase of (α_2/α_1) produces a decrease in (ΔTcr) for $(0/90)_s$ and $(0/90)_3$ laminates. This increase in (α_2/α_1) produces a greater mismatch in how different plies want to expand. This mismatch directly translates into higher internal compressive stresses, which drive buckling, leading to a lower (ΔTcr).

Table 2. Normalized critical buckling temperature (ΔTcr) of cross-ply composite plate for both symmetric and antisymmetric laminates with different aspect ratios (a/b) and thicknesses (a/h).

layup	a/b	ΔTcr				
		a/h				
		4	6	10	30	100
$(0/90)_s$	1	0.2649	0.1726	0.0819	0.0108	0.0010
	3	0.3440	0.2710	0.1661	0.0288	0.0028
	6	0.4430	0.3792	0.2985	0.0917	0.0104
	8	0.5052	0.4216	0.3456	0.1385	0.0181
$(0/90)_3$	1	0.2555	0.1652	0.0778	0.0102	0.0009
	3	0.4408	0.3737	0.2722	0.0650	0.0067
	6	0.6182	0.4978	0.4074	0.1854	0.0268
	8	0.7764	0.5759	0.4555	0.2509	0.0458

Table 4 demonstrate the relation between the normalized critical buckling temperature and both orthotropy ratio (E_1/E_2) and thickness ratio (a/h). An increase in (E_1/E_2) makes the laminates much stiffer in bending. A stiffer structure can withstand higher compressive loads (thermal loads) before it becomes unstable and buckles; that is, higher (ΔTcr). Also, this behavior is shown in **Fig. 1** for different cross plies. Different buckling modes (deformed shape) of square, symmetric cross-ply $(0/90)_{4s,}$ with thickness ratio a/h=10, are drawn in **Figure 2**, which have the same behavior, resulted from other theories.

Table 3. Normalized critical temperature (ΔTcr) of cross-ply square composite plate for both symmetric and antisymmetric laminates with different thermal expansion coefficient ratio (α_2/α_1).

layup	α_2/α_1	ΔTcr				
		a/h				
		4	6	10	30	100
$(0/90)_s$	4	1.3177	0.8583	0.4074	0.0539	0.0050
	6	1.1694	0.7617	0.3616	0.0478	0.0044
	8	1.0511	0.6846	0.3250	0.0430	0.0040
	10	0.9545	0.6217	0.2951	0.0391	0.0036
$(0/90)_3$	4	1.2711	0.8217	0.3870	0.0509	0.0047
	6	1.1280	0.7292	0.3434	0.0452	0.0042
	8	1.0139	0.6554	0.3087	0.0406	0.0037
	10	0.9207	0.5952	0.2803	0.0369	0.0034

Table 4. Normalized critical temperature (ΔTcr) of cross-ply square composite plate for different orthotropy (E_1/E_2).

layup	a/h	ΔTcr				
		E_1/E_2				
		10	**15**	**25**	**30**	**40**
(0/90)	4	0.1782	0.1893	0.2036	0.2081	0.2134
	10	0.0403	0.0443	0.0506	0.0532	0.0575
	20	0.0107	0.0119	0.0138	0.0146	0.0160
	100	0.0004	0.0005	0.0006	0.0006	0.0007
$(0/90)_2$	4	0.2233	0.2445	0.2624	0.2649	0.2636
	10	0.0597	0.0727	0.0917	0.0987	0.1088
	20	0.0165	0.0207	0.0277	0.0306	0.0354
	100	0.0007	0.0009	0.0012	0.0013	0.0016
$(0/90)_4$	4	0.2357	0.2596	0.2793	0.2819	0.2803
	10	0.0645	0.0796	0.1014	0.1093	0.1205
	20	0.0180	0.0229	0.0311	0.0345	0.0401
	100	0.0007	0.0010	0.0013	0.0015	0.0018

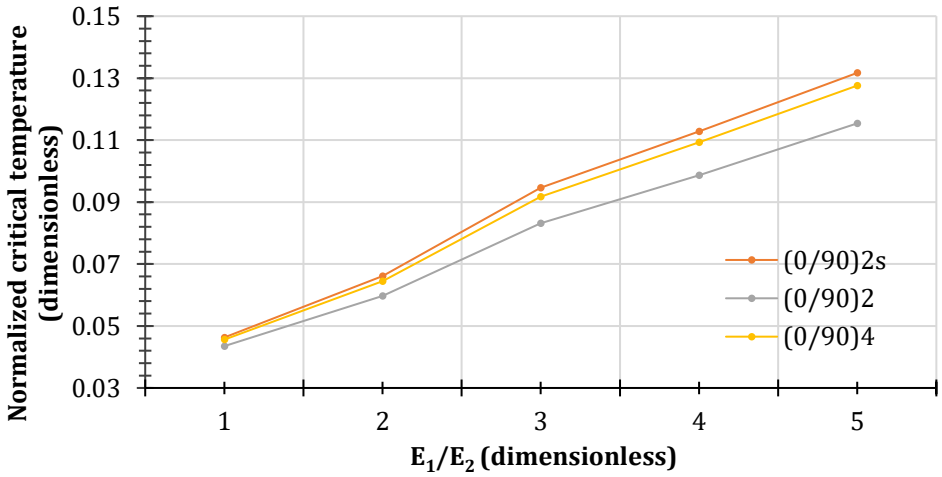

Figure 1. Normalized critical buckling temperature ($\Delta Tcr=T^*\alpha_0$) for symmetric and antisymmetric cross-ply plates for different orthotropy ratios (E_1/E_2) using material 3 and thickness a/h=10.

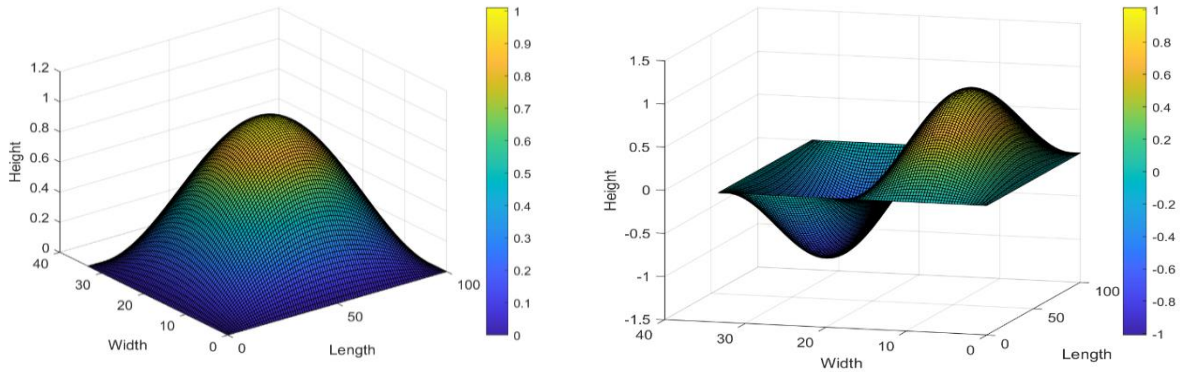

(a) First mode (m=1, n=1) (b) Second mode (m=1, n=2)

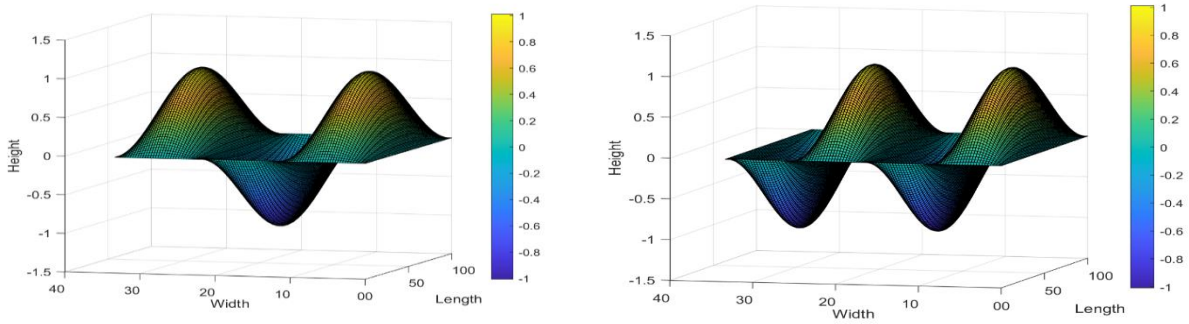

(c) Third mode (m=1, n=3) (d) Fourth mode (m=1, n=4)

Figure 2. Thermal buckling mode of square plate, symmetric cross-ply $(0/90)_{4s}$, a/h=10.

3.1.3 Angle-Ply Composite Plates

The analysis of normalized critical buckling temperature ($\Delta Tcr=T^*\alpha_0*10^3$) using material 2 for (**Table 5 and 6**) of antisymmetric angle-ply composite plates is performed in this section. In **Table 5**. critical buckling temperature of square antisymmetric angle-ply (45/-45) with a thickness ratio of (a/h=10) is calculated for various values of thermal expansion coefficient ratio, results showed inverse relation between (α_2/α_1) and (ΔTcr), the present work results also showed less than ($2.78*10^{-3}$%) discrepancy as compared with TOST **(Lee, 1997)** and good agreement with other theories, while calculating (ΔTcr) based on various values of modulus (E_1/E_2) ratio, and comparing results with other theories was conducted in **Table 6**. (ΔTcr) of moderate thickness (a/h=10) antisymmetric laminate plate results showed a direct relation between (ΔTcr) and (E_1/E_2), which is physically correct as the higher stiffness influenced by increased (E_1/E_2) causes an increase in (ΔTcr). Results of the present work compared with TOST show a maximum discrepancy of (0.00243%).

Table 5. Normalized critical buckling temperature (ΔTcr) of antisymmetric $(45/-45)_3$ simply supported square composite plate. **(Lee, 1997**; **Yahea and Majeed, 2021)**

α_2/α_1	LWT[1]	TOST[2]	RPT (13×13)	TSDT[3]	Present	Discrepancy *10^{-3}%	DQ results		
							GRT (9×9)		
							P=3 (TOT)	P=5	P=7
1	9.3134	10.3868	10.385	10.3877	10.3867	0.96	10.387	10.471	10.564
5	8.0703	9.0003	8.9991	9.0011	9.0002	1.11	9.0003	9.0730	9.1537
10	6.9163	7.7134	7.7123	7.714	7.7133	1.30	7.7133	7.7757	7.8448
20	5.3782	5.998	5.9972	5.9985	5.9979	1.67	5.9980	6.0465	6.1002
30	4.3998	4.9068	4.9062	4.9072	4.9067	2.04	4.9068	4.9464	4.9904
40	3.7225	4.1515	4.151	4.1519	4.1515	0	4.1515	4.1851	4.2223
50	3.226	3.5978	3.5973	3.598	3.5977	2.78	3.5977	3.6268	3.6591

Table 6. Normalized critical temperature (ΔTcr) for various values of modulus ratio (E_1/E_2) for antisymmetric angle-ply $(45/-45)_3$ square laminate composite plate. **(Lee, 1997**; **Yahea and Majeed, 2021)**

E_1/E_2	LWT[1]	TOST[2]	RPT (13×13)	TSDT[3]	Present	Discrep-ancy *10-3 %	DQ results GRT (9×9)		
							P=3 (TOST)	P=5	P=7
2	2.4672	2.4721	2.4721	2.4722	2.4721	0	2.4721	2.4744	2.4771
5	4.6703	4.7728	4.7728	4.7730	4.77284	0.84	4.7728	4.7823	4.7928
10	8.1229	8.5390	8.5386	8.5391	8.53899	0.12	8.5390	8.5697	8.6029
15	11.507	12.352	12.3509	12.3518	12.3517	2.43	12.3517	12.413	12.4799
20	14.954	16.309	16.3079	16.3094	16.3090	0	16.3090	16.409	16.5195
30	22.482	25.073	25.0700	25.0756	25.0732	0.8	25.0733	25.2756	25.5007
40	31.711	35.904	35.8980	35.9117	35.9040	0	35.9041	36.2438	36.6308
50	44.290	50.684	50.6737	50.7028	50.6839	0.2	50.6840	51.2138	51.8351

Dimensionless critical buckling temperature ($\Delta Tcr=T^*\alpha_0$) of an antisymmetric ten-layer simply supported composite plate of material 3 is shown in **Table 7**. Various values of thickness ratios and fiber angles were taken into account for comparing (ΔTcr) evaluated based on the present theory and compared with previous theories, showing a maximum discrepancy of (13.09%) when compared with 3D[1] **(Noor and Burton, 1992)** and good agreement with other theories. The maximum value of (ΔTcr) appears at (**θ** =45).

Table 7. Dimensionless buckling temperature (ΔTcr) of square simply supported antisymmetric $(\theta/-\theta)_5$ angle-ply composite plate. **(Noor and Burton, 1992**; **Babu and Kant, 2000**; **Matsunaga, 2006**; **Yahea and Majeed, 2021)**

a/h	θ	3D[1]	TOT[2]	GHOT[3]	TSDT[4]	Present	Discrepancy %	GRT P=7
100	0	7.463*10-4	7.470*10-4	7.463*10-4	7.469*10-4	7.4697*10-4	0.09	7.466*10-4
	15	1.115*10-3	1.116*10-3	1.115*10-3	1.1159*10-3	1.1159*10-3	0.08	1.115*10-3
	30	1.502*10-3	1.502*10-3	1.502*10-3	1.502*10-3	1.5023*10-3	0.02	1.502*10-3
	45	1.674*10-3	1.675*10-3	1.675*10-3	1.675*10-3	1.6750*10-3	0.06	1.675*10-3
20	0	1.739*10-2	-	1.739*10-2	1.773*10-2	1.7729*10-2	1.95	1.757*10-2
	15	2.528*10-2	-	2.531*10-2	2.59*10-2	2.5906*10-2	2.48	2.562*10-2
	30	3.446*10-2	-	3.456*10-2	3.477*10-2	3.4771*10-2	0.90	3.484*10-2
	45	3.81*10-2	-	3.826*10-2	3.844*10-2	3.8438*10-2	0.89	3.859*10-2
10	0	5.782*10-2	5.778*10-2	5.782*10-2	6.127*10-2	6.1250*10-2	5.93	5.963*10-2
	15	7.904*10-2	7.920*10-2	7.933*10-2	8.481*10-2	8.4779*10-2	7.26	8.211*10-2
	30	0.1100	0.1108	0.1110	0.1130	0.112984	2.71	0.1137
	45	0.1194	0.1208	0.1209	0.1225	0.122478	2.58	0.1240
20/3	0	0.1029	-	0.1029	0.1125	0.112412	9.24	0.1081
	15	0.1322	-	0.1330	0.1468	0.146637	10.92	0.1399
	30	0.1859	-	0.1888	0.1942	0.194005	4.36	0.1958
	45	0.1981	-	0.2023	0.2065	0.206253	4.12	0.2101
5	0	0.1436	0.1417	0.1436	0.1593	0.159112	10.80	0.1524
	15	0.1753	0.1746	0.1765	0.1979	0.197465	12.64	0.1874
	30	0.2377	0.2421	0.2432	0.2604	0.259755	9.28	0.2575
	45	-	0.2651	0.2656	0.2728	0.272072	-	0.2777
4	0	0.1777	-	0.1777	0.1980	0.197419	11.10	0.1893

	15	0.2087	-	0.2103	0.2370	0.236027	13.09	0.2239
	30	-	-	0.2754	0.3105	0.309211	-	0.2922
	45	-	-	0.3114	0.3221	0.320564	-	0.3266
10/3	0	0.2057	-	0.2057	0.2287	0.227717	10.70	0.2190
	15	0.2347	-	0.2367	0.2668	0.265114	12.96	0.2518
	30	-	-	0.2988	0.3413	0.337603	-	0.3170
	45	-	-	0.3443	0.3592	0.356640	-	0.3614

Table 8 demonstrate the effect of both aspect ratio (a/b) and thickness ratio (a/h) on normalized critical buckling temperature ($\Delta Tcr=T^*\alpha_0$) of antisymmetric laminate plates [(45/-45)2, (45/-45)3] using material 3, as the thickness ratio (a/h) increases critical temperature decrease due to thickness reduction, on the other hand Increase in aspect ratio (a/b) causes increase in (ΔTcr), while buckling temperature comparison between angle and cross plates is shown in **Fig. 3**.

Table 8. Normalized critical buckling (ΔTcr) temperature of antisymmetric laminate composite plate for various aspect ratios (a/b) and thickness ratios (a/h).

Lay up	a/ b	ΔTcr			
		a/h			
		4	10	20	100
$(45/-45)_2$	1	0.300352	0.110221	0.033973	0.001469
	2	0.371143	0.183217	0.066577	0.003119
	3	0.416061	0.244054	0.103787	0.005373
	4	0.453709	0.293141	0.143665	0.008375
$(45/-45)_3$	1	0.313338	0.118319	0.036927	0.001605
	2	0.383853	0.194093	0.071819	0.003399
	3	0.428967	0.255853	0.111058	0.005838
	4	0.467693	0.305075	0.152618	0.009080

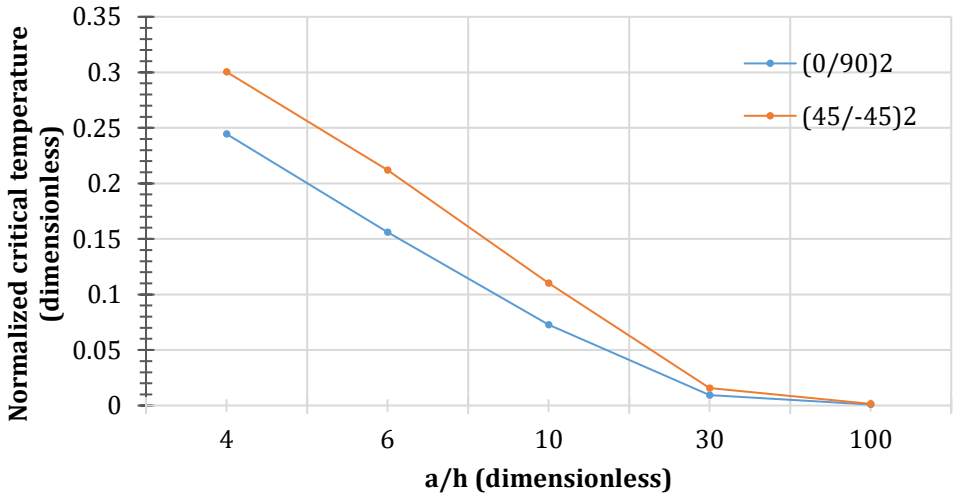

Figure 3. Normalized critical buckling temperature ($\Delta Tcr=T^*\alpha_0$) for cross-ply $(0/90)_2$ and angle-ply $(45/-45)_2$ plates for different thickness (a/h) values using material 3.

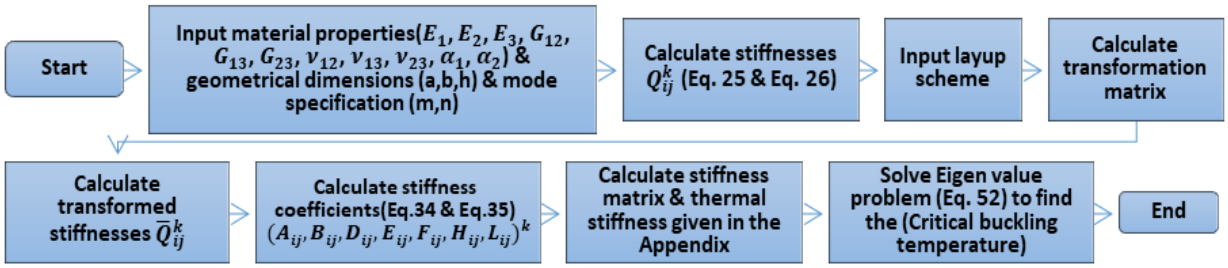

Figure 4. Flow chart for computer programming to calculate critical buckling temperature.

4. CONCLUSIONS

This study introduces, for the first time, a refined hyperbolic shear deformation theory to analyze the thermal buckling of simply-supported cross-ply and angle-ply laminated plates d. The theory uses a four-variable displacement field with a hyperbolic function to accurately represent transverse shear strain across the thickness, eliminating the need for a shear correction factor. Based on Hamilton's principle and solved via Navier's method, the model's results are validated against other shear deformation theories. The numerical findings demonstrate that this new theory excels at predicting the critical buckling load of laminated plates, showing good agreement with more complex higher-order models. Another conclusion is that the thermal buckling resistance is not an inherent property of the constituent materials alone but is a complex, coupled function of the laminate's stacking sequence, the number of layers, and the orthotropic characteristics of the material, as expected. The key findings can be summarized as follows:

- Increasing the number of layers (increasing thickness) naturally increases (ΔTcr) for a fixed thickness. Laminates with a greater number of thinner plies (allowing for more refined angle transitions) offered a performance advantage over those with fewer.
- Symmetric laminates consistently outperform antisymmetric ones by eliminating detrimental bending-extension coupling, leading to higher critical buckling temperatures.
- Angle-ply schemes $(\theta/-\theta)_n$ often provide superior, tunable buckling resistance compared to cross-ply $(0/90)_n$, by aligning fibers with the dominant thermal stress.
- A high fiber-direction stiffness (E_1) and a low coefficient of thermal expansion (α_1) are key. The material's anisotropy (E_1/E_2) dictates the optimal stacking sequence and the higher critical temperature.

NOMENCLATURE

Symbol	Description	Symbol	Description
a, b	Plate length and width (m)	N_{xx},N_{yy} ,N_{xy}	membrane forces (N/m)
A_{ij},B_{ij},D_{ij},E_{ij}, F_{ij},H_{ij},L_{ij}	Stiffness terms (N/m)	N^T_{xx},N^T_{yy}, N^T_{xy}	Thermally induced membrane forces (N/m)
E_1,E_2,E_3	Youngs modulus (GPa)	w_b,w_s	displacement in bending, shear, respectively
h	Plate thickness (m)	x,y,z	Coordinate axes
k	Number of plate layers	ε_x, ε_y, ε_z	Strain components (m/m)
M^b_{xx},M^b_{yy}, M^b_{xy}	Bending moment per unit length (N.m/m)	γ_{yz},γ_{xz}	Transverse shear strain (m/m)
M^s_{xx}, M^s_{yy}, M^s_{xy}	Moment per unit length due to shear (N.m/m)	$\sigma_{ij(x,y,z)}$	Stress components (GPa)
Q_y, Q_x	Transverse shear force (N)	ν_{12}, ν_{12}	Poison's ratio

Acknowledgements

This work was supported by the Mechanical Engineering Department, College of Engineering, University of Baghdad.

Credit Authorship Contribution Statement

Ahmed K. Sabea: Writing –review & editing, Writing – original draft, Validation, Software, Methodology. Widad I. Majeed: Supervising and following up on the research.

Declaration of Competing Interest

The authors declare that they have no known competing financial interests or personal relationships that could have appeared to influence the work reported in this paper.

REFERENCES

Abdulrazzaq, M.A., Fenjan, R.M., Ahmed, R.A., Faleh, N.M., 2020. Thermal buckling of nonlocal clamped exponentially graded plate according to a secant function based refined theory. *Steel Compos. Struct*, 35(1), pp. 147-157. https://doi.org/10.12989/scs.2020.35.1.149.

Anandan, G., Gopalan, V., Natarajan, S., 2022. Thermal buckling of flax fibre reinforced epoxy laminated composite plate using finite element analysis. *International Journal for Computational Methods in Engineering Science and Mechanics*, 23(3), pp. 219-227. https://doi.org/10.1080/15502287.2021.1948149.

Babu, C.S., Kant, T., 2000. Refined higher order finite element models for thermal buckling of laminated composite and sandwich plates. *Journal of Thermal Stresses*, 23(2), pp. 111-130. https://doi.org/10.1080/01.4957300280489

Bracaglia, F., Masia, R., Pagani, A., Zappino, E., Carrera, E., 2024. Thermal buckling of variable stiffness composite laminates using high order plate finite elements. *Composite Structures*, 345, P. 118393. https://doi.org/10.1016/j.compstruct.2024.118393.

Daikh, A.A., Bachiri, A., Houari, M.S.A., Tounsi, A., 2020. Size dependent free vibration and buckling of multilayered carbon nanotubes reinforced composite nanoplates in thermal environment. *Mechanics Based Design of Structures and Machines*, 50(4), pp. 1371-1399. https://doi.org/10.1080/15397734.2020.1752232.

Devarajan, B., Kapania, R.K., 2022. Analyzing thermal buckling in curvilinearly stiffened composite plates with arbitrary shaped cutouts using isogeometric level set method. *Aerospace Science and Technology*, 121, P. 107350. https://doi.org/10.1016/j.ast.2022.107350.

Ebrahimi, F., Nopour, R., Dabbagh, A., 2021. Effect of viscoelastic properties of polymer and wavy shape of the CNTs on the vibrational behaviors of CNT/glass fiber/polymer plates. *Engineering with Computers*, 38(S5), pp. 4113-4126. https://doi.org/10.1007/s00366-021-01387-7.

Elsisi, A., Abdel-Monsef, S., Salim, H., 2025. Artificial Intelligence in the Design and Optimization of Laminated FRP Composites: A Review of Methodologies and Applications. *Journal of Composites Science*, 9(12), P. 654. https://doi.org/10.3390/jcs9120654.

Hajlaoui, A., Dammak, F., 2022. A modified first shear deformation theory for three-dimensional thermal post-buckling analysis of FGM plates. *Meccanica*, 57(2), pp. 337-353. https://doi.org/10.1007/s11012-021-01427-y.

Hashim, H.A., Sadiq, I.A., 2021. A five-variable refined plate theory for thermal buckling analysis of composite plates. *Compos. Mater. Eng*, 3(2), pp. 135-155. https://doi.org/10.12989/cme.2021.3.2.135.

Kada, D., Abdelouahed, T., 2022. A new refined hyperbolic shear deformation theory for laminated composite spherical shells. *Structural engineering and mechanics: An international journal*, 84(6), pp. 707-722. https://doi.org/10.12989/sem.202.2.84.6.707

Kareem, M.G., 2024. Thermal buckling analysis for hybrid and composite laminated plate by using new displacement function. *Open Engineering*, 14(1), https://doi.org/10.1515/eng-2022-0597

Khandan, R., Noroozi, S., Sewell, P., Vinney, J., 2012. The development of laminated composite plate theories: a review. *Journal of Materials Science*, 47(16), pp. 5901-5910. https://doi.org/10.1007/s10853-012-6329-y.

Lee, J., 1997. Thermally induced buckling of laminated composites by a layerwise theory. *Computers & Structures*, 65(6), pp. 917-922. https://doi.org/10.1016/S0045-7949(96)00232-5.

Li, D., Zhu, H., Gong, X., 2021. Buckling analysis of functionally graded sandwich plates under both mechanical and thermal loads. *Materials*, 14(23), P. 7194. https://doi.org/10.3/390ma14237194.

Ma, R., Jin, Q., 2022. Stability of functionally graded graphene-reinforced composite laminated thick plates in thermal environment. *Acta Mechanica*, 233(10), pp. 3977-3996. https://doi.org/10.1007/s00707-022-03300-9.

Majeed, W.I., Sadiq, I.A., 2022. Thermal buckling of laminated plates using modified Mantari function. *J Mech Eng*, 19(3), pp. 205-220.

Majeed, W.I., Sadiq, I.A., 2025. Buckling Analysis of Composites Plates Using Four Variable Refined Plate Theory. *Revue des Composites et des Materiaux Avances*, 35(3), P. 567. https://doi.org/10.18280/rcma.350317.

Matsunaga, H., 2006. Thermal buckling of angle-ply laminated composite and sandwich plates according to a global higher-order deformation theory. *Composite Structures*, 72(2), pp. 177-192 . https://doi.org/10.1016/j.compstruct.2004.11.016.

Mehditabar, A., Ansari Sadrabadi, S., Walker, J., 2023. Thermal buckling analysis of a functionally graded microshell based on higher-order shear deformation and modified couple stress theories. *Mechanics Based Design of Structures and Machines*, 51(5), pp. 2812-2830. https://doi.org/10.1080/15397734.2021.1908145.

Miglani, J., Devarajan, B., Kapania, R.K., 2022. Isogeometric thermal buckling and sensitivity analysis of periodically supported laminated composite beams. *AIAA Journal*, 60(5), pp. 3215-3224. https://doi.org/10.2514/1.J060814.

Moradi Haghighi, S., Alibeigloo, A., 2023. Thermal buckling and vibrational analysis of carbon nanotube reinforced rectangular composite plates based on third-order shear deformation theory. *Journal of Engineering Mechanics*, 149(6), P. 04023026. https://doi.org/10.1061/JENMDT.EMENG-6875.

Nguyen, T.-K., Thai, H.-T., Vo, T.P., 2020. A novel general higher-order shear deformation theory for static, vibration and thermal buckling analysis of the functionally graded plates. *Journal of Thermal Stresses*, 44(3), pp. 377-394. https://doi.org/10.1080/01495739.2020.1869127.

Noor, A.K., Burton, W.S., 1992. Three-dimensional solutions for thermal buckling of multilayered anisotropic plates. *Journal of Engineering Mechanics*, 118(4), pp. 683-701. https://doi.org/10.1061/(ASCE)0733-9399(1992)118:4.(683)

Odeh, A., Al-Shugaa, M.A., Al-Gahtani, H.J., Mukhtar, F., 2024. Analysis of laminated composite plates: a comprehensive bibliometric review .*Buildings*, 14(6), pp. 1574. https://doi.org/10.3390/buildings14061574.

Qian, H., Wang, Z., Lu, C., Cai, D., Yang, Y., 2024. Thermal analysis for laminated plates with arbitrary supports under non-uniform temperature boundary conditions. *Thin-Walled Structures*, 197, P. 111595. https://doi.org/10.1016/j.tws.2024.111595.

Reddy, J.N., 2003. *Mechanics of laminated composite plates and shells: theory and analysis*. CRC press..

Saad, M., Hadji, L., 2022. Thermal buckling analysis of porous FGM plates. *Materials Today: Proceedings*, 53, pp. 196-201. https://doi.org/10.1016/j.matpr.2021.12.550.

Shu, X., Sun, L., 1994. Thermomechanical buckling of laminated composite plates with higher-order transverse shear deformation. *Computers & Structures*, 53(1), pp. 1-7. https://doi.org/10.1016/0045-7949(94)90123-6.

Torabi, J., Ansari, R., Hassani, R., 2019. Numerical study on the thermal buckling analysis of CNT-reinforced composite plates with different shapes based on the higher-order shear deformation theory. *European Journal of Mechanics-A/Solids*, 73, pp. 144-160. https://doi.org/10.1016/j.euromechsol.2018.07.009.

Varelis, D., Saravanos, D.A., 2022. A coupled nonlinear plate finite element for thermal buckling and postbuckling of piezoelectric composite plates including thermo-electro-mechanical effects. *Journal of Thermal Stresses*, 45(1), pp. 30-50. https://doi.org/10.1080/01495739.2021.2005498.

Xing, Y., Wang, Z., 2017. Closed form solutions for thermal buckling of functionally graded rectangular thin plates. *Applied Sciences*, 7(12), P. 1256. https://doi.org/10.3390/app7121256.

Xue, Y., Zhang, Y., Li, J., 2021. Optimization of thermal buckling control for composite laminates with PFRC actuators using trigonometric shear deformation theory. *Journal of Mechanical Science and Technology*, 35(1), pp. 257-266. https://doi.org/10.1007/s12206-020-1225-x.

Yahea, H.T., Majeed, W.I., 2021. Thermal buckling of laminated composite plates using a simple four variable plate theory. *Journal of Engineering*, 27(9), pp. 1-19 . https://doi.org/10.31026/j.eng.2021.09.01.

Yang, X., Fei, Q., Wu, S., Li, Y., 2020. Thermal buckling and dynamic characteristics of composite plates under pressure load. *Journal of Mechanical Science and Technology*, 34(8), pp. 3117-3125. https://doi.org/10.1007/s12206-020-0702-6.

Appendix

1. *Stiffness matrix elements for cross-ply laminates:*

$$K_{11} = (A_{11}\alpha^2 + A_{66}\beta^2) \quad , \quad K_{12} = (A_{12} + A_{66})\alpha\beta$$
$$K_{13} = -(B_{11}\alpha^3 + (B_{12} + 2B_{66})\alpha\beta^2) \quad , \quad K_{14} = -(E_{11}\alpha^3 + (E_{12} + 2E_{66})\alpha\beta^2)$$
$$K_{22} = (A_{66}\alpha^2 + A_{22}\beta^2), K_{23} = -(B_{22}\beta^3 + (B_{12} + 2B_{66})\alpha^2\beta)$$
$$K_{24} = -(E_{22}\beta^3 + (E_{12} + 2E_{66})\alpha^2\beta)$$
$$K_{33} = (D_{11}\alpha^4 + 2(D_{12} + 2D_{66})\alpha^2\beta^2 + D_{22}\beta^4)$$
$$K_{34} = (F_{11}\alpha^4 + 2(F_{12} + 2F_{66})\alpha^2\beta^2 + F_{22}\beta^4)$$
$$K_{44} = (H_{11}\alpha^4 + 2(H_{12} + 2H_{66})\alpha^2\beta^2 + H_{22}\beta^4 + L_{55}\alpha^2 + L_{44}\beta^2)$$
$$A_{16} = A_{26} = B_{16} = B_{26} = D_{16} = D_{26} = E_{16} = E_{26} = F_{16} = F_{26} = H_{16} = H_{26} = L_{45} = 0$$

2. *Stiffness matrix elements for Angle-ply laminates:*

$$K_{11} = (A_{11}\alpha^2 + A_{66}\beta^2), K_{12} = (A_{12} + A_{66})\alpha\beta$$
$$K_{13} = -(3B_{16}\alpha^2\beta + B_{26}\beta^3), K_{14} = -(3A_{16}\alpha^2\beta + E_{26}\beta^3)$$
$$K_{22} = (A_{66}\alpha^2 + A_{22}\beta^2), K_{23} = -(B_{16}\alpha^3 + 3B_{26}\alpha\beta^2)$$
$$K_{24} = -(E_{16}\alpha^3 + 3E_{26}\alpha\beta^2)$$
$$K_{33} = (D_{11}\alpha^4 + 2(D_{12} + 2D_{66})\alpha^2\beta^2 + D_{22}\beta^4)$$
$$K_{34} = (F_{11}\alpha^4 + 2(F_{12} + 2F_{66})\alpha^2\beta^2 + F_{22}\beta^4)$$
$$K_{44} = (H_{11}\alpha^4 + 2(H_{12} + 2H_{66})\alpha^2\beta^2 + H_{22}\beta^4 + L_{55}\alpha^2 + L_{44}\beta^2)$$
$$A_{16} = A_{26} = B_{11} = B_{12} = B_{22} = B_{66} = D_{16} = D_{26} = E_{11} = E_{12} = E_{22} = E_{66} = F_{16} = F_{26} = H_{16} = H_{26} = L_{45} = 0$$

تحليل الانبعاج الحراري للصفائح المركبة الرقائقية باستخدام نظرية الصفائح المُطَوَّرة ذات المتغيرات الأربعة

احمد خميس سبع*، وداد إبراهيم مجيد

قسم الهندسة الميكانيكية، كلية الهندسة، جامعة بغداد، بغداد، العراق

الخلاصة

تبحث هذه الورقة البحثية دراسة الانبعاج الحراري للصفائح المركبة الرقائقية بناءاً على الإطار النظري لنظرية الصفائح المُطَوَّرة ذات المتغيرات الأربعة. باستعمال دالة تشوه قصي جديدة وغير مسبوقة في تحليل الانبعاج الحراري للصفائح المدعمة ببساطة على جميع الحواف. تجمع دالة القص المكونة من دوال القطع الزائد والدوال متعددة الحدود بين محاكاة تغير اجهاد القص المستعرض عبر سمك الصفيحة وتحقيق شرط انعدام الاجهاد على السطح المستعرض العلوي والسفلي للصفيحة، دون الحاجة الى استخدام معامل التصحيح القصي. تم اشتقاق معادلات الحركة وفقاً لمبدأ الازاحة الافتراضية، وتم تنفيذ الحل التحليلي باستخدام حل "نافير" الذي يستوفي شروط التدعيم البسيط، كما تم حساب النتائج العددية للخصائص المتباينة لكل من الصفائح ذات الترتيب المتقاطع والترتيب الزاوي من خلال صياغة تشفير لبرنامج "MATLAB".في هذه الدراسة، تم تحليل تأثير تغيير معاملات التصميم المختلفة مثل نسبة العرض الى الارتفاع (a/b)، نسبة معامل التمدد الحراري (α_2/α_1)، نسبة السماكة (a/h)، ونسبة تباين الخواص (E_1/E_2) للصفائح المركبة الرقائقية المتناظرة وغير المتناظرة. واظهرت النتائج تطابقا جيداً لكل من الصفائح السميكة والرقيقة مقارنة بالدراسات السابقة.

الكلمات المفتاحية: الانبعاج الحراري، الصفائح المركبة، نظرية القص المُطَوَّرة.